

# Modeling and Validation of 48V Mild Hybrid Lithium-Ion Battery Pack

**SoDuk Lee, Jeff Cherry, Michael Safoutin, Joseph McDonald, and Michael Olechwi,**  
U.S. Environmental Protection Agency, USA

## Abstract

As part of the midterm evaluation of the 2022-2025 Light-Duty Vehicle Greenhouse Gas (GHG) Standards, the U.S. Environmental Protection Agency (EPA) developed simulation models for studying the effectiveness of 48V mild hybrid electric vehicle (MHEV) technology for reducing CO<sub>2</sub> emissions from light-duty vehicles. Simulation and modeling of this technology requires a suitable model of the battery. This article presents the development and validation of a 48V lithium-ion battery model that will be integrated into EPA's Advanced Light-Duty Powertrain and Hybrid Analysis (ALPHA) vehicle simulation model and that can also be used within Gamma Technologies, LLC (Westmont, IL) GT-DRIVE™ vehicle simulations. The battery model is a standard equivalent circuit model with the two-time constant resistance-capacitance (RC) blocks. Resistances and capacitances were calculated using test data from an 8 Ah, 0.4 kWh, 48V (nominal) lithium-ion battery obtained from a Tier 1 automotive supplier, A123 Systems, and developed specifically for 48V mild hybrid vehicle applications. The A123 Systems battery has 14 pouch-type lithium-ion cells arranged in a 14 series and 1 parallel (14S1P) configuration. The RC battery model was validated using battery test data generated by a hardware-in-the-loop (HIL) system that simulated the impact of MHEV operation on the A123 systems 48V battery pack over U.S. regulatory drive cycles. The HIL system matched charge and discharge data originally generated by Argonne National Laboratory (ANL) during chassis dynamometer testing of a 2013 GM Chevrolet Malibu Eco 115V MHEV. All validation testing was performed at the battery test facility (BTF) at the U.S. EPA National Vehicle and Fuel Emissions Laboratory (NVFEL) in Ann Arbor, Michigan. The simulated battery voltages, currents, and state of charge (SOC) of the HIL tests were in good agreement with vehicle test data over a number of different drive cycles, and excellent agreement was achieved between RC model simulations of the 48V battery and HIL battery test data.

## Keywords

48V Lithium Ion Battery, HIL Tests, RC Model Validation

## Citation

Lee, S., Cherry, J., Safoutin, M., McDonald, J. et al.,  
"Modeling and Validation of 48V Mild Hybrid Lithium-Ion Battery Pack," *SAE Int. J. Alt. Power.* 7(3):273-287, 2018,  
doi:10.4271/2018-01-0433.

This article is based on and revised or modified from a presentation at WCX18, Detroit, MI, April 10-12, 2018.

## Introduction

The introduction of 48-volt (48V) mild hybrid electric vehicles (MHEVs) has stimulated development of 48V battery systems capable of providing enhanced driving performance, higher energy density battery packs, and the improved life cycle durability required by consumers and necessary for full-useful-life compliance with U.S. emissions standards. Much of this activity has involved the development of advanced lithium-ion chemistries and in some cases development of variations of deep-cycle lead-acid chemistries such as lead-carbon formulations [1].

Mild hybrid vehicles with 48V systems have recently appeared in the European light-duty vehicle market due to high fuel prices and stringent new European Union CO<sub>2</sub> passenger car emissions standards. Renault introduced the 2017 model year Scenic and Grand Scenic, which are 48V MHEV diesel multi-purpose vehicles (MPVs) using a 10 kW electric machine and a 48V lithium-ion battery originally developed by Continental [2]. The Scenic is approximately 8 to 10% more efficient when using the 48V MHEV system. Mercedes-Benz introduced a low cost, 12 kW belt starter-alternator (BSA or P0) 48V MHEV system and a 15 kW engine integrated starter-alternator (ISA or P1) 48V MHEV system with an electrically driven charge air boosting system for their E-class and S-class sedans, respectively [3, 4]. An approximately 20 to 23% fuel efficiency was realized via engine downsizing, friction reduction, accessory electrification, and 48V MHEV operation (e.g., torque assist and brake recovery). Audi recently announced introduction of a 48V MHEV system for the Audi A8 [5], and FCA has introduced 48V P0 MHEV systems branded as “eTorque” on North American versions of the Jeep Wrangler SUV and RAM 1500 pickup truck [6].

The Advanced Light-Duty Powertrain and Hybrid Analysis (ALPHA) tool was developed by EPA to model vehicle performance, fuel economy, greenhouse gas (GHG) emissions, and battery pack performance for light-duty conventional and hybrid electric vehicles (HEV) [7]. ALPHA can be used as a support tool for future GHG emissions regulations or as a research tool to evaluate the efficiency of new advanced vehicle technologies. The hybrid model within ALPHA is related to EPA’s heavy-duty vehicle Greenhouse Gas Emissions Model (GEM) [8] certification tool. Light-duty ALPHA vehicle simulations use the same basic sub-models and controls as heavy-duty vehicle GEM simulations with the exception of specific traction motors, generators, batteries, regenerative braking controls, hybrid vehicle supervisory controls (VSC), etc. that differ somewhat between light-duty and heavy-duty applications.

Within MHEV, HEV, and plug-in hybrid electric vehicle (PHEV) applications, an analysis of the battery pack performance, state-of-charge (SOC) trajectory optimization, and optimization of electric motor/internal combustion engine power coupling is of importance since the overall efficiency of the vehicle is closely tied to the efficiency of the battery pack and the energy flows through the hybrid drive system. A two-time constant equivalent circuit battery cell model was

developed to closely simulate lithium-ion battery pack voltages. The estimated voltage was then used to calculate traction motor and generator current by dividing it from motor power. The motor power was calculated by multiplying motor torque and motor speed estimated from VSC. A lumped capacitance battery thermal model was developed to determine battery pack temperature. To rapidly achieve an optimum battery pack temperature of 25 to 40°C, battery management system (BMS) thermal control strategies such as cabin-air heating and variable airflow rates were also implemented within the model.

The battery pack model enables fuel economy and GHG emissions to be estimated by simulating the effects of battery cell power capacity, SOC operating window, discharge and charge power limits (PL), battery pack temperatures, battery cell internal resistance, and BMS thermal control strategies.

## Battery Pack Tests

The 0.4 kWh, 48V, 8 Ah LiFePO<sub>4</sub> battery pack used for testing and simulated during battery modeling was provided by A123 Systems (Livonia, MI, USA) (Table 1 and Figure 1). The battery pack was tested at the EPA National Vehicle and Fuel Emissions Laboratory (NVFEL) battery test facility (BTF) to characterize the resistance, capacitance, charge, and discharge behavior of the battery pack.

An AeroVironment AV-900 battery cyler (AeroVironment, Inc., Monrovia, CA, USA) was used to provide the demanded power/current to and from the 48V battery pack for the initial 10-second discharging and charging pulse tests and to follow specific charge/discharge cycles to simulate battery function during vehicle operation. The battery cyler, cooling systems, and control systems used at the NVFEL BTF allow “hardware-in-the-loop” (HIL) operation that provides a close approximation of battery operating conditions that would exist within a vehicle chassis during operation over vehicle regulatory drive cycles such as the urban dynamometer driving schedule (UDDS) and the highway fuel economy test (HwFET) (Figure 2). Input data for HIL operation was based upon chassis dynamometer testing of a 2013 GM Chevrolet Malibu Eco by Argonne National Laboratory that was conducted as part of the U.S. Department of Energy-Vehicle Technologies Office Advanced Vehicle Testing Activity [9, 10, 11]. The Malibu Eco is equipped with a 115V belt integrated

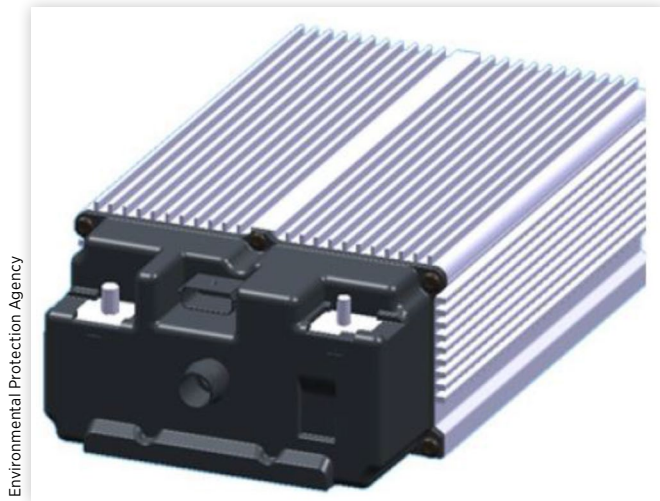
**TABLE 1** 48V lithium-ion battery pack specifications.

Battery pack make/model	A123 Systems, LiFePO <sub>4</sub> “UltraPhosphate”
Battery pack serial no.	522702V04C17G1800022
Rated capacity/energy	8 Ah/384 Wh
Size (L × W × H)	304 mm × 180 mm × 96 mm
Mass	8 kg
Topology	14S1P

Environmental Protection Agency

Created by Environmental Protection Agency.

**FIGURE 1** A123 Systems 0.4 kWh 8 Ah 48V lithium-ion battery pack.



Environmental Protection Agency

starter generator (BISG or P0) MHEV system. The battery BMS control area network (CAN) communication bus provided battery pack voltages ( $V_{Batt}$ ), battery pack currents ( $I_L$ ), and battery pack temperatures at 20 Hz/50 ms transmission rates during the tests.

The battery manufacturer provided the open-circuit voltage (OCV) curves for the cells, as shown in Figure 3. PL were implemented using a two-dimensional look-up table to estimate the effects of SOC and cell/pack temperatures.

Both the charge and discharge power limits (DPL) are reduced to zero when the battery pack temperature is above 65°C or below -30°C, temperatures that represent the upper and lower operating limits for this particular cell chemistry. As shown in Figure 4, the desired operating temperature of the battery is between 20°C and 55°C although battery operation can be briefly extended to between -30°C and 65°C. The maximum allowable charging and discharging PL of the 48V battery pack are 16 kW and 15 kW, respectively, at 50% SOC and a 25°C battery pack temperature near the beginning-of-life.

The BMS has a self-balancing SOC control function. At -30°C, the battery can still discharge at approximately 30 A for 10 seconds at 50% SOC, which is sufficient to crank the engine for cold starts. The 10-second discharging and

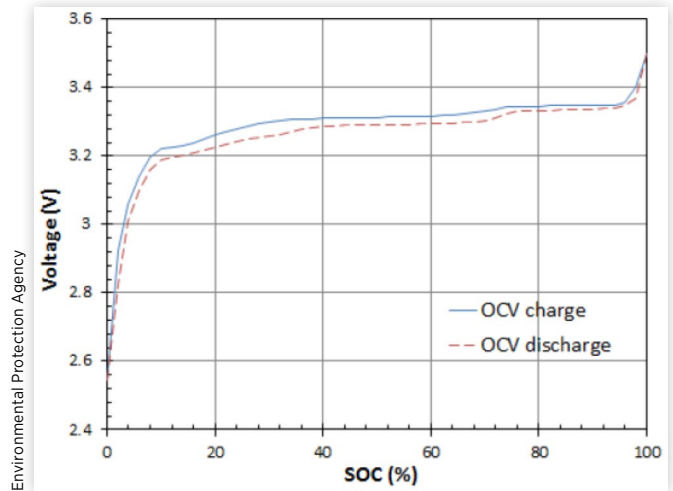
**FIGURE 2** Battery test setup at EPA NVFEL BTF.



Environmental Protection Agency

Created by Environmental Protection Agency.

**FIGURE 3** Open-circuit voltage ( $V_{OC}$ ) of A123 Systems lithium-ion battery cell at 23°C.



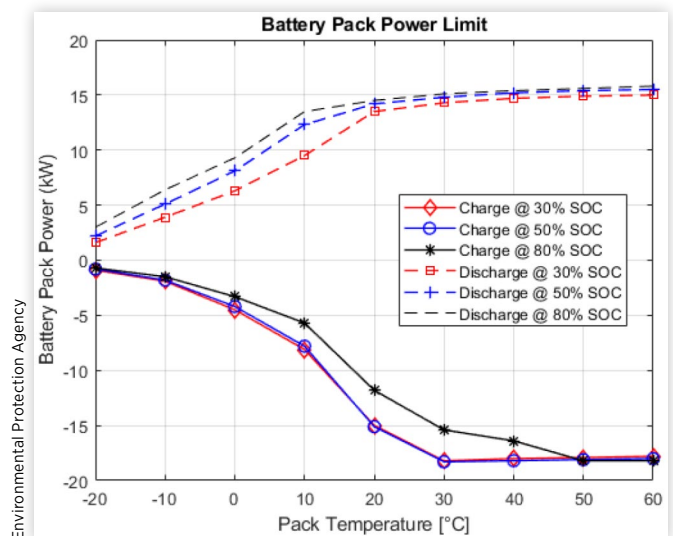
Environmental Protection Agency

charging current limits are approximately 370 A between 30% SOC and 60% SOC and for pack temperatures between 30 and 60°C.

Figure 5 shows that the demanded current (blue line) from the AV900 battery cycler has an approximately 100~200 ms delay in order to reach the requested current (red line) at the battery terminals. The battery pulse currents achieved were offset from the demanded current due to CAN-based data transmission rates that are limited to 10 Hz/100 ms.

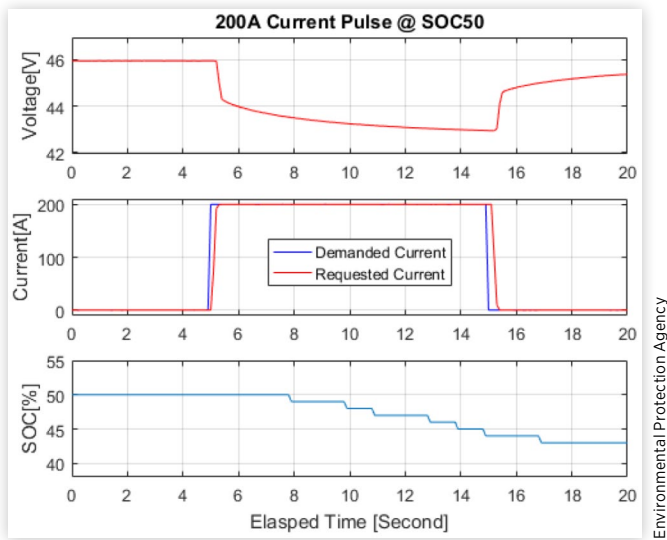
The ohmic series, short-, and long-time resistances and capacitances were calculated by using 10-second current pulse test data. As shown in Figure 6, the time constant for the short-time resistances and capacitances ( $\tau_{ST}$ ) was calculated by taking the time from the start of the pulse test to the point where the blue-colored curve intersects with a 45° line from

**FIGURE 4** 10-second PL for the 48V lithium-ion battery pack.



Environmental Protection Agency

**FIGURE 5** 200A10 second discharging pulse test.



the horizontal (shown by the dashed red line). The short-time capacitance and resistance ( $R_{ST}$  and  $C_{ST}$ , respectively) and long-time capacitance and resistance ( $R_{LT}$  and  $C_{LT}$ , respectively) can be calculated by estimating cell voltage recovery response gradients [12] when running high I-V (current-voltage) discharging and charging current pulse tests at various SOC levels. The  $R_{LT}$  and the long-time interval time constant ( $\tau_{LT}$ ) were calculated from voltage changes ( $\Delta V$ )/battery current ( $I_L$ ) and the test time taken from the intersection point between blue-colored curve and the dashed red line to the end of the 10-second I-V pulse tests, respectively. Long-time capacitances ( $C_{LT}$ ) were calculated by  $\tau_{LT}/R_{LT}$ . A typical lithium-ion battery charging efficiency of 98~99% and typical heat capacity and heat convection coefficients were based upon values in published literature [15, 16, 17, 18].

**FIGURE 6** A time constant ( $\tau$ ) for short-/long-time resistance and capacitance.

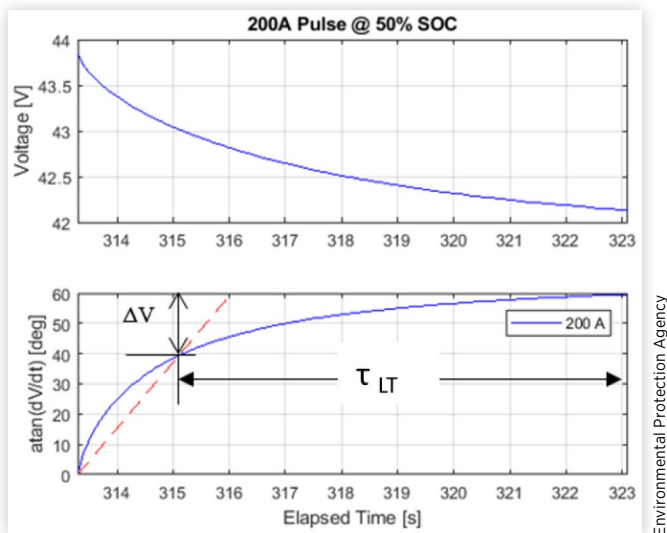
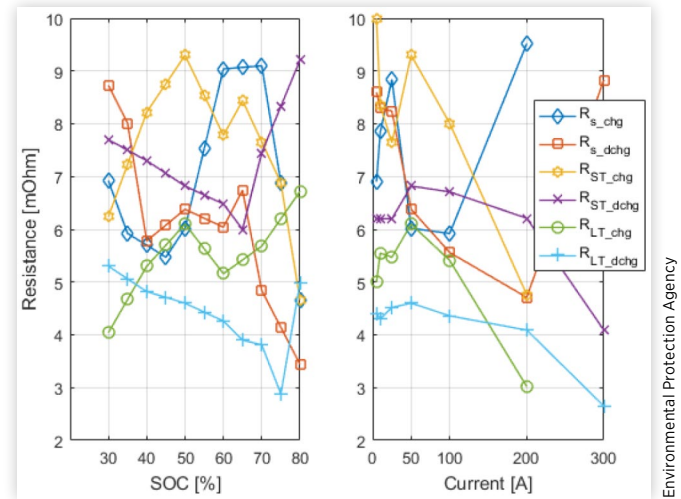


**FIGURE 7** Ohmic resistances of 48V 14 Cell Lithium-Ion Battery Pack.



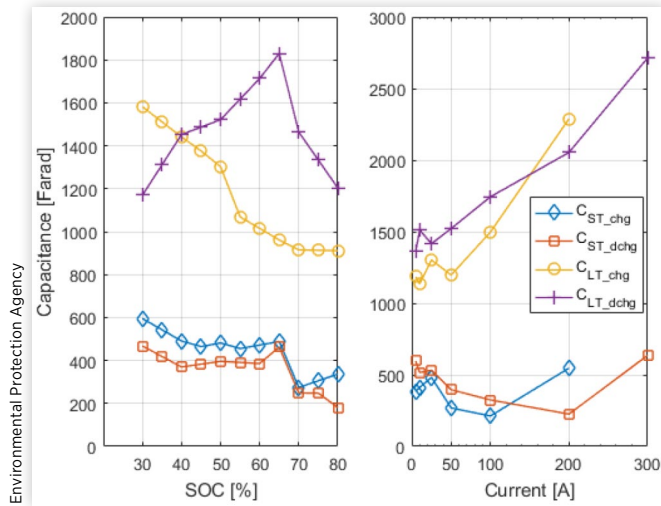
Note that voltage response gradients from battery pack I-V tests may be different from the voltage response gradients of battery cell I-V tests due to cell-to-cell SOC imbalance and cell-to-cell voltage variations.

As shown in Figure 7, the measured battery pack ohmic series, short-, and long-time resistances and capacitances are significantly reduced compared to those of typical lithium-ion battery packs in order to maintain battery pack voltages within the desired voltage range between 36V and 52V, even during very high current discharging and charging events. The measured 8 to 10 milliohm ( $m\Omega$ ) ohmic resistance of this pack was low, suggesting optimization for 48V MHEV applications. The measured ohmic series, short-, and long-time resistances for the pack were used as inputs for MATLAB/Simulink look-up tables to estimate the effects of SOC and the 10-second charging/discharging current pulse tests.

The charging pulse tests using 5, 10, 25, 50, 100, and 200 A currents were conducted at 20, 30, 40, 50, 60, and 70% SOC in order to prevent charging above 80% SOC, which is the manufacturer's recommended upper SOC window limit. A 300 A current was not used in the charging pulse test since it rapidly reaches the battery SOC limit. On the other hand, discharging pulse tests using 5, 10, 25, 50, 100, 200, and 300 A were performed at 80, 70, 60, 50, 40, and 30% SOC in order to prevent discharging below the recommended 20% SOC lower limit. The " $R_s$ ," " $R_{ST}$ ," and " $R_{LT}$ " are series ohmic, short-time, and long-time resistances, respectively. The detailed ohmic resistances, short- and long-time resistances, and capacitances of the 48V battery pack tested at various SOC and current levels are presented in Appendix B.

As shown in Figure 7, ohmic series charging and discharging resistances generally increased while short- and long-time charging/discharging resistances decreased at higher current. Hence, battery resistance was dependent on both SOC and battery current. The 50 A charging and discharging pulse current and 50% SOC were used to plot

**FIGURE 8** Capacitances of 48V 14 Cell Lithium-Ion Battery Pack.

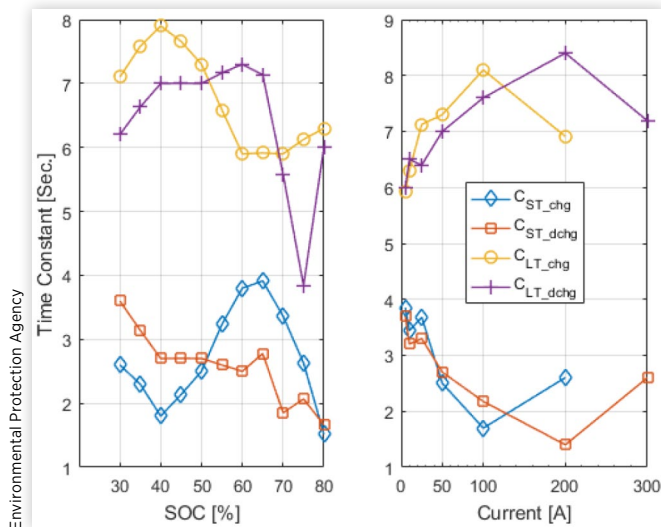


Figures 7, 8, and 9 for referencing the 47.2 A RMS and 48.1 A RMS pack currents for the UDDS and HwFET drive-cycle HIL test data as shown in Figures 13 and 15, respectively. The “chg” and “dchg” subscripts in the figures designate charging and discharging current pulse events.

As shown in Figures 8 and 9, the short-time charging and discharging capacitances and time constants are lower than the long-time charging and discharging capacitances and time constants at various SOC and current levels.

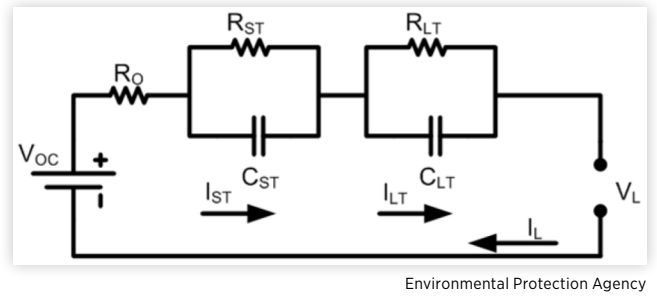
In automotive 48V MHEV applications, the lower nominal voltage 48V battery pack experiences higher discharging and charging current than previous higher-voltage MHEV pack designs, such as the 115V system used with the Malibu Eco MHEV, when delivering or receiving the same electric power to and from the vehicle.

**FIGURE 9** Time constants of 48V 14 Cell Lithium-Ion Battery Pack.



Created by Environmental Protection Agency.

**FIGURE 10** Battery equivalent circuit cell model.



## Battery Pack Model

The battery pack model in ALPHA consists of an equivalent circuit cell model, a battery thermal model, and BMS controls. Accurate SOC, discharge power, and charge PL are required to estimate available traction motor power and torque precisely.

## Equivalent Circuit Cell Model

A two-time constant equivalent circuit model [13, 14, 15] was applied to calculate terminal voltages for a lithium-ion polymer cell. Battery pack voltages were calculated by multiplying the number of cells in series within the battery pack.

In Figure 10, the  $V_{OC}$  is the OCV of a cell.  $R_O$  is the ohmic resistance of a cell and is dependent on the SOC and cell and pack temperatures.  $R_{ST}$  and  $C_{ST}$  are resistances and capacitances of the electro-magnetic short-time double layer effects, respectively.  $R_{LT}$  and  $C_{LT}$  are resistances and capacitances of the electro-chemical long-time mass transport effects, respectively.  $I_L$  is the cell load current. Discharge current is positive while negative current represents charging.

Battery cell terminal voltage,  $V_L$ , can be calculated by using a typical RC circuit equation 1:

$$V_L = V_{OC} + I_L * R_O + \int (I_L - I_{ST})/C_{ST} dt + \int (I_L - I_{LT})/C_{LT} dt \quad \text{Eq. (1)}$$

where  $I_{ST} = V_{ST}/R_{ST}$  and  $I_{LT} = V_{LT}/R_{LT}$ .

Battery pack voltage,  $V_{Batt}$ , was calculated using Equation 2:

$$V_{Batt} = V_L * N_{series} / N_{parallel} \quad \text{Eq. (2)}$$

where  $N_{series}$  is 14 cells with series connections and  $N_{parallel}$  is 1 parallel connection for this particular 48V pack. Battery pack voltages,  $V_{Batt}$ , and battery pack currents,  $I_L$ , were obtained from the vehicle CAN communication bus during vehicle chassis dynamometer testing. The 48V battery pack was tested at a complete pack level, and therefore the wiring harness and bus bar effects are already included when measuring battery pack resistances and capacitances from the 48V battery pack terminals.

## Battery Thermal Model

The lumped capacitance battery thermal model [15, 16, 17] in ALPHA was developed to provide battery pack temperature information to a battery voltage control block, battery PL control block, and BMS control strategies.

The battery pack temperature was calculated in Equation 3 by using the energy balance between battery heat generation,  $Q_{ees\_gen}$ , and heat loss,  $Q_{ees\_cooling}$  while also considering the thermal mass of the battery pack and the method of cooling:

$$T_{ees} = \int_0^t \frac{(Q_{ees\_gen} - Q_{ees\_cooling})}{m_{ees} C_{p,ees}} dt + T_0 \quad \text{Eq. (3)}$$

where  $m_{ees}$  is the mass of the battery pack electric energy storage system,  $T_0$  is the initial pack temperature, and  $C_{p,ees}$  is battery heat capacity [16, 17, 18, 19].

In Equation 4, the charging efficiency is Coulombic efficiency. Coulombic charge efficiencies of 99, 98, and 97% were used at below 85%, between 85% and 90%, and above 90% SOC levels, respectively. The  $Q_{ees\_gen}$  is calculated by Equation (4):

$$Q_{ees\_gen} = I_L * R_{Batt}^2 + (1 - \text{Coulombic charge efficiency}) * I_L * V_{Batt} \quad \text{Eq. (4)}$$

The battery pack resistance,  $R_{Batt}$ , is obtained using Equation 5:

$$R_{Batt} = (R_O + R_{ST} * I_{ST}/I_L + R_{LT} * I_{LT}/I_L) * N_{series}/N_{parall} \quad \text{Eq. (5)}$$

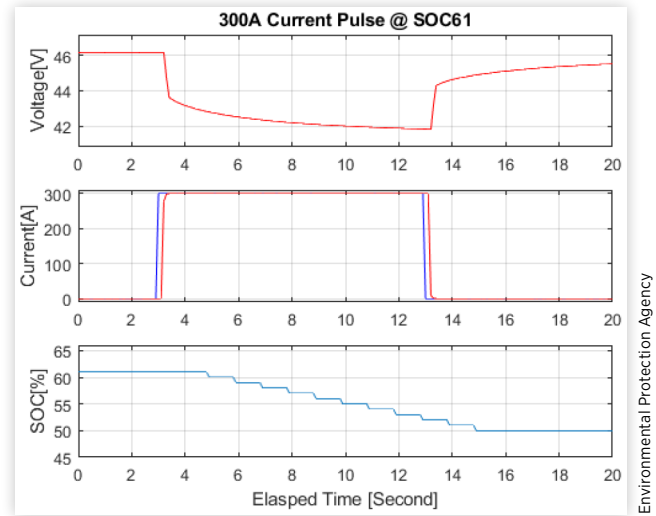
where  $R_O$  is battery cell discharging or charging resistance. The cell resistance,  $R_O$ , is estimated by using a two-dimensional discharge look-up table when battery current is positive and by using the charging resistance when battery current is negative. The battery terminal voltage,  $R_{Batt}$ , is also a function of time due to the time-dependent capacitance in the two-time constant equivalent circuit battery model as shown in Figures 5 and 12. The battery life and aging effects were not considered at this time due to insufficient aged 48V battery pack field test data.

The  $Q_{ees\_cooling}$ , is calculated by using Equation 6:

$$Q_{ees\_cooling} = (h A_s + kt)(T_{ees} - T_{coolant}) \quad \text{Eq. (6)}$$

where  $T_{coolant}$  is the battery pack inlet coolant temperature, which can be the temperature of the ambient air, the cabin-conditioned air, or the liquid water coolant depending on the battery cooling system design.  $A_s$  is the battery surface area for convection heat transfer, and  $t$  is the thickness of the battery pack for heat transfer via conduction. A typical battery conduction coefficient,  $k$ , and convection coefficient,  $h$ , were found in published references [16, 17, 18]. The lumped thermal equations were implemented by using MATLAB/Simulink blocks. The specifications from Table 1 and Figure 11 were used to validate the battery model within ALPHA.

**FIGURE 11** A 300 ampere discharging current pulse test at 60% SOC.



## Battery Management System Controls

Battery cooling control strategies were also implemented to emulate typical HEV BMS cooling controls. With sufficient cooling, the pack temperature can be decreased to the cooling OFF temperature, and the cooling ON strategy can be reactivated after the pack temperature rises to the specified cooling ON temperature. The cooling ON/OFF temperature settings can be calibrated for typical vehicle operating conditions such as operation in regions with hot and cold temperatures. There is no active battery cooling when the pack temperature is below 25°C, and an active battery heating system may be required when the pack temperature is extremely low under cold ambient conditions. The tested A123 Systems 48V battery pack was not equipped with active cooling. Instead, it uses passive air cooling with aluminum fins and has a vent for expelling battery gases in the event of a cell failure. Hence, passive air cooling was used during model validation.

The available DPL was calculated using Equation 7:

$$DPL_{avail} = DPL(SOC(t)) - DPL(\text{minimum SOC}) \quad \text{Eq. (7)}$$

where  $DPL_{avail}$  is the available DPL,  $DPL(SOC)$  is the discharge power limit at a given SOC, and the minimum SOC is 30%. The typical SOC maximum in MHEVs is 80%, and the maximum, high, low, and minimum values of the SOC windows can be calibrated to optimize battery cell performance and cell durability for MHEV applications. The battery pack can provide sufficient electric power to a P0 (e.g., BISG) or inline P2 (e.g., clutched/transmission-integrated) traction motor when the required road-load power is less than the available DPL. The available discharge power is used to turn on the internal combustion engine if the demanded road-load power is greater than the available discharge power. The battery DPL vary depending on pack temperature and SOC level.

For final SOC balancing, the following proportional-integral-derivative (PID) controller algorithm was employed during model simulation:

$$\begin{aligned} \Delta \text{Power}_{\text{Batt}} &= \text{PL}(\text{SOC}(t)) - \text{PL}(\text{SOC}_{\text{target}}) \\ \text{Power}_{\text{comp}} &= \Delta \text{Power}_{\text{Batt}} + k_p \Delta \text{SOC}(t) + k_i \int \Delta \text{SOC}(t) dt \\ &\quad + k_d \frac{d}{dt} \Delta \text{SOC}(t) \end{aligned} \quad \text{Eq. (8)}$$

$$\begin{aligned} \Delta \text{SOC}(t) &= \text{SOC}(t) - \text{SOC}_{\text{target}}, \quad k_p = 15.7, \\ k_i &= 3.5, \quad k_d = 0.018 \end{aligned}$$

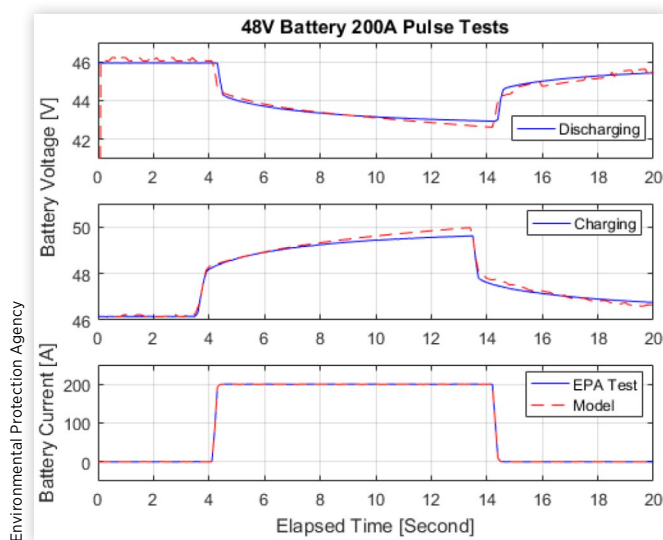
where PL is the discharge and charge power limit for positive current and for negative current, respectively.

## Battery Model Validation

Figure 11 shows that the pack can maintain the desired battery voltage levels between 36V and 52V under 300 A high current pulse tests although the battery pack SOC was reduced by approximately 10 % during the 10-second pulse test.

As shown in Figure 12, the simulated discharging and charging battery pack voltages are in good agreement with the 48V battery test data. The root-mean-squared (RMS) voltage differences between the simulated discharging and charging pack voltage and the RMS voltage differences of the test data are within 0.11V during a 200 A 10-second pulse test. The simulated voltage was quickly recovered by completing the discharging current pulse, and the pack voltage during the 48V lithium-ion battery pack tests returned slowly to the OCV. The measured 45.05V RMS and the modeled 45.07V RMS pack voltages were within 0.1% for the 200 A discharging pulse test. The modeled 46.93V RMS pack voltage differed by less than 0.3% relative to the measured 47.04V RMS pack voltage for the 200 A charging pulse test. Hence, the modeled and measured charging and discharging voltages were in good agreement.

**FIGURE 12** Discharging/charging pulse tests at 50% SOC.

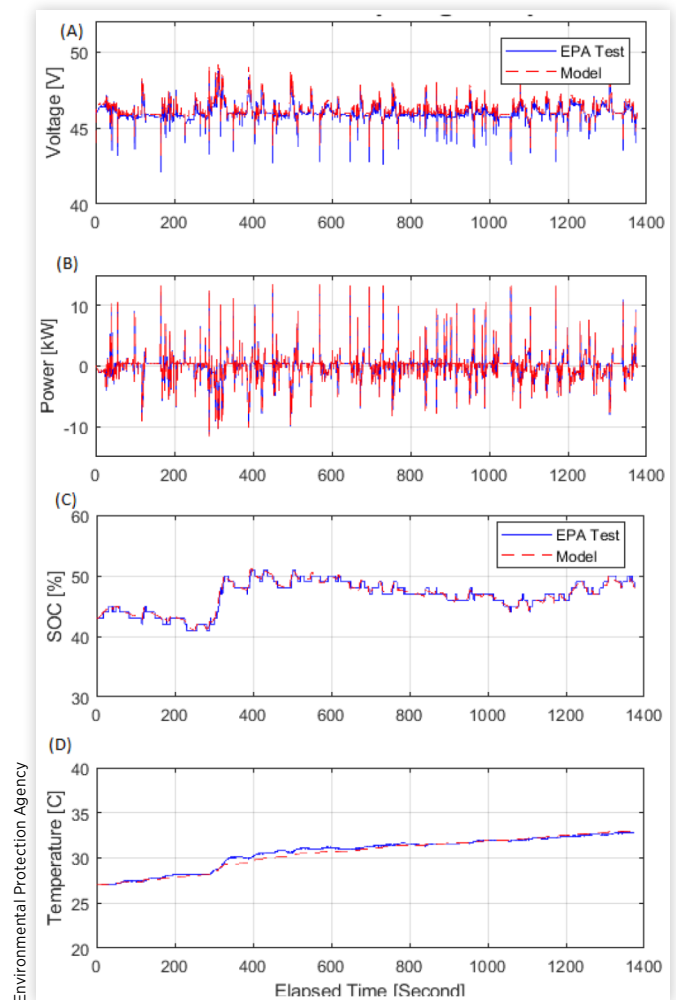


Created by Environmental Protection Agency.

Modeled and HIL-measured battery pack RMS voltage, power, SOC, and temperature over the UDDS cycle are compared in Figure 13. The RMS voltage differences between the simulated voltages and the HIL test data shown were approximately 0.8V RMS, and the simulated voltage averages were within 0.7% of the HIL test data averages over the UDDS driving cycle (Figure 13A).

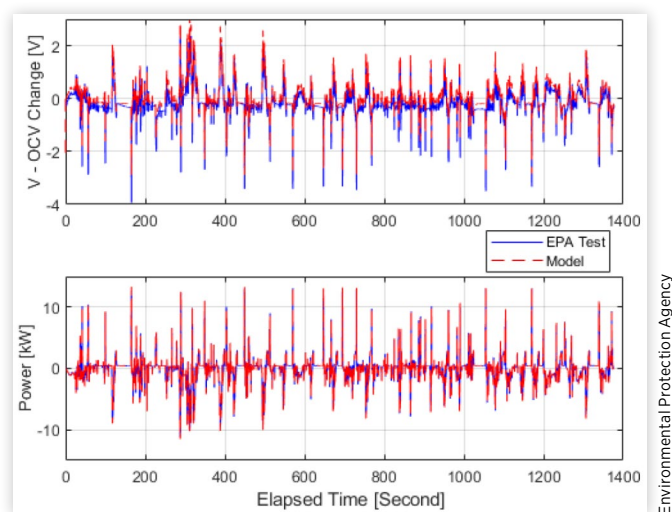
The modeled 48V battery pack power and SOC were in good agreement with the HIL test data (Figure 13B and C). The captured RMS regenerative braking energy differences between the modeled 48V battery pack and those of the HIL battery test data were within 0.12 kW. Modeled battery pack temperatures (Figure 13D) were also in excellent agreement with HIL battery test data. The modeled 46.2V RMS and the measured 46.01V RMS battery pack voltages over the HIL simulation of the UDDS cycle were in good agreement. The modeled 30.58°C RMS temperatures and the measured 30.71°C RMS pack temperatures were also in an excellent

**FIGURE 13** Modeled (red) and measured (blue) power (A), voltage (B), SOC (C), battery temperature (D) for a 48V lithium-ion battery pack during HIL simulation of the UDDS cycle.



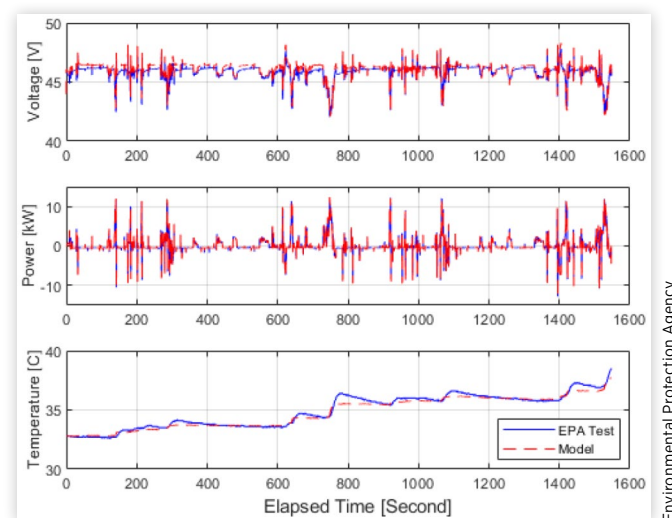
Environmental Protection Agency

**FIGURE 14** Modeled (red) and measured (blue) voltage changes (V-OCV) for a 48V lithium-ion battery pack during the UDDS cycle.



Environmental Protection Agency

**FIGURE 15** Modeled (red) and measured (blue) voltages and temperatures for the 48V battery during HIL simulation of the two HwFET cycles.



Environmental Protection Agency

agreement, and the pack temperature was increased about 6°C over the HIL UDDS simulation test when using the 2013 Malibu Eco chassis dynamometer test battery charge and discharge power profiles. The battery pack can maintain the desired voltage levels between 36 and 52V at a current of 47.2 A RMS during the UDDS driving cycle.

As shown in Figure 14, the modeled 0.5535V RMS voltage changes were within 1.3% of the measured 0.5609V RMS voltage changes from the battery pack OCV to the battery pack terminal voltage ( $V_{\text{Batt}} - \text{OCV}$ ) during the UDDS drive cycle. Hence, the measured and the modeled voltage changes due to ohmic series, short-, and long-time resistances and capacitances in the two-time constant equivalent circuit model are in good agreement.

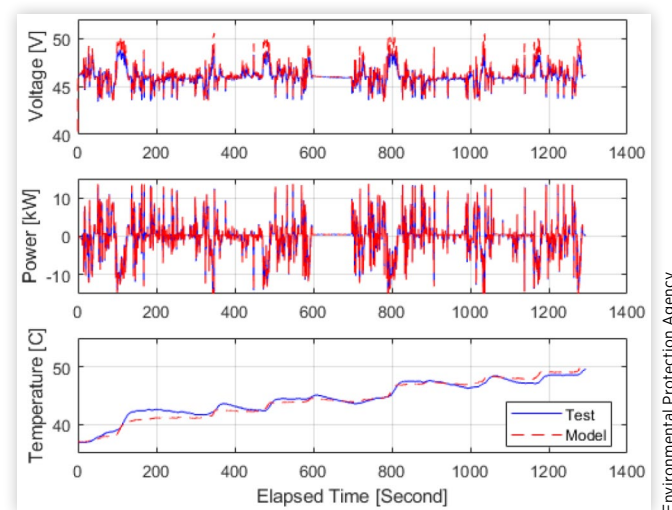
As shown in the first plot in Figure 15, the battery pack can also hold the desired operating voltage levels between 36 and 52V at a current of 48.1 A RMS during the HwFET driving cycle. The modeled 46.03V and 48.1 A RMS pack voltage and current and the 45.87V and 48.1 A RMS pack voltages and current measured during HIL battery testing over the HwFET were in good agreement.

A 795 J/kg-K specific heat capacity [16, 17] and 18.9 W/m<sup>2</sup>-K heat transfer coefficient [18] for the battery pack and a 0.25 W/m-K thermal conductivity for the case material served as inputs into the thermal model. The temperature surrounding the battery pack was assumed to be approximately 30°C during testing at the BTF when calculating heat conduction from or to the battery pack. The modeled 34.81°C RMS temperatures and the measured 34.95°C RMS pack temperatures were in excellent agreement. As shown in Figure 15, the instantaneous battery temperatures from the test data and model simulations are also in very good agreement.

As shown in the first plot in Figure 16, the battery pack can still hold the desired operating voltage levels between 36 and 52V at a current of 88.2 A RMS during operation over the

higher speeds, loads, and accelerations represented in the US06 driving cycle [20]. The modeled 46.19V and 88.2 A RMS voltage and current and the HIL-measured 46.04V and 88.2 A RMS voltage and current are in very good agreement. The modeled 44.36°C RMS pack temperatures and the measured 44.56°C RMS pack temperatures were in an excellent agreement. The pack temperature was increased approximately 12.7°C from the initial 37°C pack temperature during HIL testing when using charge/discharge data from chassis dynamometer testing of the Malibu Eco MHEV over the US06 cycle. Even assuming passive cooling, the pack was able to maintain pack temperatures within an acceptable operating range for operation over two consecutive US06 drive cycles.

**FIGURE 16** Modeled (red) and measured (blue) voltages and temperatures for the 48V battery during HIL simulation over two consecutive US06 cycles separated by 100 seconds of idle.



Environmental Protection Agency

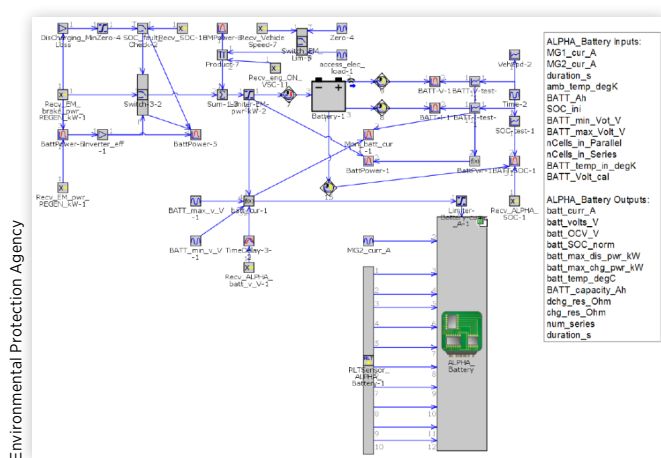
Resistances and capacitance are generally dependent on battery pack temperatures. Batteries cannot be operated beyond their specified temperature operating limits, such as extremely low and high temperatures. High-precision thermal chambers and extensive testing time would be required to test battery packs at various pack temperatures, which was beyond the scope of this study. In this study, the 48V lithium-ion battery was tested at laboratory temperatures of approximately 20°C to validate the battery model at temperatures consistent with vehicle chassis dynamometer testing for EPA emissions and fuel economy compliance. The available battery power was calculated using the manufacturer's battery pack PL at battery pack temperatures from -20 to 60°C and various SOC levels as shown in [Figure 4](#).

## Battery and Vehicle Model Co-Simulations

As shown in [Figure 17](#), the Gamma Technology GT-DRIVE vehicle model was used to simulate 48V MHEV models at an early conceptual stage [21]. The EPA's engine and battery models were compiled using Microsoft Visual Studio 10 and the 2016a version of the MATLAB/Simulink/Stateflow toolbox to create a dynamic link library (DLL). The ALPHA battery DLL was critical for calculating battery discharge and charge PL, battery charging efficiency, pack temperature, etc., precisely during vehicle drive-cycle simulations. A smart utilization of battery power is of paramount importance for any vehicle electrification application and for proper modeling of vehicle GHG emissions and fuel consumption.

A DLL was developed specifically to simulate the A123 Systems lithium-ion battery cell used within the 48V MHEV battery pack, and the DLL was used to build a GT-DRIVE simulation of a 48V BISG (P0) MHEV version of the Malibu Eco MHEV [21]. This vehicle was originally equipped with a higher-voltage, 0.5 kWh 4.4 Ah 32 cell 115V lithium-ion battery pack and 12/15 kW (discharge/charge) BISG MHEV system.

**FIGURE 17** Schematic of the GT-Suite Battery and ALPHA Battery Model DLL (a larger version is reproduced within the Appendix for purposes of readability).



Created by Environmental Protection Agency.

**FIGURE 18** Engine speed and engine state of 2013 GM Malibu Eco over the UDDS.

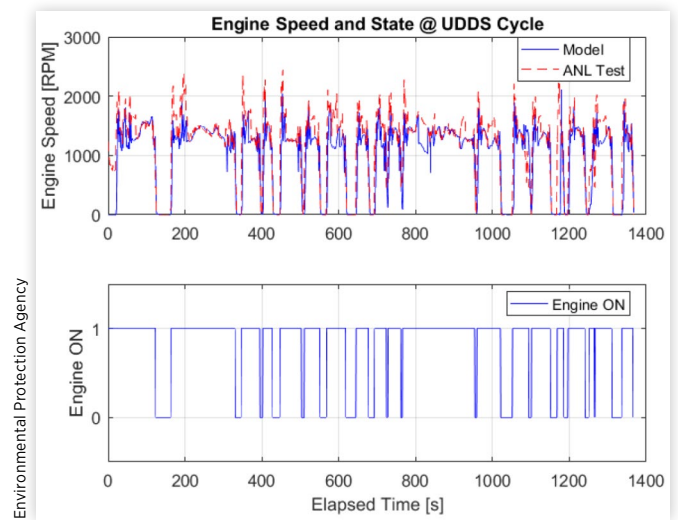
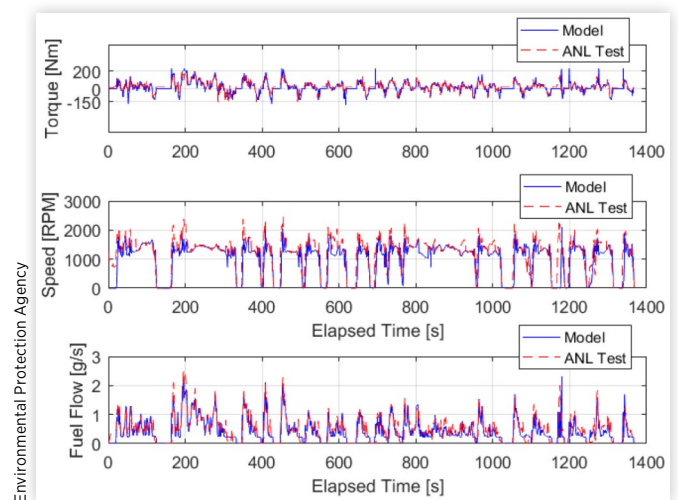


[Figure 18](#) shows that the 1071 seconds of engine-on time from the 48V MHEV model simulation was in excellent agreement with the 1070 seconds of engine-on time from the ANL test data for the Malibu Eco MHEV over the UDDS [10, 11]. Therefore, the simulated engine-on time and the engine-on time of the test data were comparable when using the available discharge battery PL.

As shown in [Figure 19](#), the simulated engine torque for the 48V MHEV operated within a region of higher engine efficiency to minimize fuel consumption, similar to the 115V Malibu Eco MHEV test data. The trends of engine torque and speed for the GT-DRIVE 48V MHEV simulation were in good agreement with those of the 115V Malibu Eco MHEV chassis dynamometer test data [10, 11]. The 57.1 Nm RMS engine torque for the simulated 48V MHEV was within 4.5% of the

**FIGURE 19** Modeled 48V MHEV (blue) and measured 115V MHEV engine torque and fuel flow over the UDDS.



Created by Environmental Protection Agency.

54.7 N-m RMS engine torque 115V Malibu Eco MHEV test data [22, 23]. Overall, the simulated engine torque and speed shown in Figure 19 were in good agreement with the engine torque and speed from the chassis dynamometer test data provided by ANL.

The estimated motor current and accessory current were used as inputs into the battery pack model to estimate the battery pack SOC and voltage. Charge efficiencies and battery pack temperature were also considered when estimating the battery pack SOC.

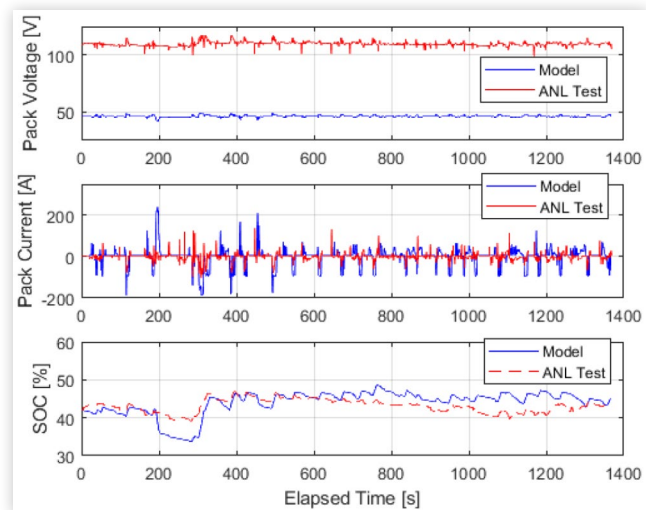
As shown in Figure 20, the 42.7 A RMS current for the 48V MHEV was significantly higher when compared to the 17.9 A RMS current for the 115V Malibu Eco MHEV test data over the UDSS [10, 11] due to the battery pack voltage change from 115V to 48V. The simulated final SOC of the 48V battery pack had lower discharged battery power and higher final SOC than what was found during the ANL UDSS tests of the 115V MHEV version of the vehicle and thus represented conservative estimations with respect to GHG emissions. The SOC swing windows of the modeled 0.4 kWh 48V battery pack are greater than the SOC windows of the original equipment manufacturer (OEM) 0.5 kWh 2013 Malibu Eco 115V battery pack since the SOC varies more quickly due to the reduced storage capacity of the 48V pack when charging and discharging the same electric power when compared to the higher-capacity and higher-voltage OEM 115V battery pack.

In Table 2, fuel economy (mpg) and GHG emission (g CO<sub>2</sub>/km) can be calculated by using Equations 9, 10, respectively:

$$\text{Fuel economy} = \text{VMT}_{\text{mile}} / m_{\text{gallon}} \quad \text{Eq. (9)}$$

$$\text{GHG emission (gCO}_2 / \text{km)} = \rho \times m_{\text{liter}} \times \psi \times (44 / 12) / \text{VMT}_{\text{km}} \quad \text{Eq. (10)}$$

**FIGURE 20** Modeled 48V MHEV (blue) and measured 115V MHEV battery pack voltage, current, and SOC over the UDSS.



Environmental Protection Agency

**TABLE 2** UDSS and HwFET cycle fuel economy of 48/115V MHEVs.

Driving cycle	Initial/final SOC (%)	CO <sub>2</sub> (g/km)	Fuel economy (mpg)	Remark
115V UDSS/w 0.5 kWh	42/43.3	163.2	34.0	ANL test [10, 11]
	42/44.6	161.7	34.3	Model
48V UDSS/w 0.4 kWh	42/45.1	162.7	34.1	Model
115V HwFET/w 0.5 kWh	43/48.3	113.4	48.9	ANL test [10, 11]
	43/43.1	114.2	48.6	Model
48V HwFET/w 0.4 kWh	43/46.7	115.8	47.9	Model

Environmental Protection Agency

where  $\text{VMT}_{\text{mile}}$  and  $\text{VMT}_{\text{km}}$  are vehicles traveled in miles and kilometers,  $m_{\text{gallon}}$  and  $m_{\text{liter}}$  are engine fuel flows in gallons and liters,  $\rho$  is fuel density (g/liter),  $\psi$  is carbon weight fractions of fuels, and 44 and 12 are from atomic masses of CO<sub>2</sub> and C, respectively. For the CO<sub>2</sub> emissions and fuel economy reported in Table 2, a fuel density of 742.45 g/liter at 15°C and a carbon weight fraction of 0.8664 were used to represent typical values for the Tier 2 E0 certification gasoline currently used for GHG and CAFE compliance.

The simulation shows that similar UDSS and HwFET cycle fuel economy and GHG emissions can be achieved (Table 2) by using a 0.4 kWh, 48V battery pack and MHEV system in place of the OEM 0.5 kWh 115V battery pack and system, with the potential for significantly reducing battery pack weight and size. Additional weight reduction could be realized by using an inverter-integrated 48V electric machine and eliminating the long three-wire, three-phase AC cables from the rear trunk area of the Malibu Eco to the BISG motor near the engine pulley location. The simulation did not consider the weight-savings from the smaller, lighter 48V lithium-ion pack, the simplification of the wiring harness, or from inverter integration into the electric machine.

The battery pack PL-based engine ON/OFF control strategy enabled fuel economy and GHG emissions to be estimated with improved precision by updating battery cell capacity, the minimum SOC set points, etc., during drive-cycle modeling runs. Increased fuel economy and GHG emission reduction could also be achieved by improving battery cell PL without changing the minimum SOC set points. This control strategy would be useful to optimize the best SOC operating window range when increasing battery cell power output via battery cell chemistry improvements, thermal management improvements, or other system design changes.

## Summary and Conclusions

A two-time constant equivalent circuit battery cell model along with a lumped capacitance thermal model and BMS

control strategies was implemented within a model of a 48V MHEV battery pack, for incorporation into the EPA ALPHA model and Gamma Technology GT-DRIVE vehicle simulations to explore various combinations of advanced future HEV technologies. Excellent agreement between battery model simulations and test data was achieved. In addition, model simulation time was significantly reduced by using simple and computationally efficient models.

The electric circuit battery model was incorporated as a DLL into a 48V MHEV model for vehicle-level drive-cycle co-simulation using the Gamma Technology GT-DRIVE model. This model was used to simulate GHG emissions and fuel economy of a BISG 48V MHEV with a second-by-second time resolution. Vehicle models such as GT-DRIVE and the EPA ALPHA model can be used to quantify the effectiveness of new advanced vehicle technologies by estimating the relative improvement in GHG emissions, fuel economy, and vehicle and battery pack performance.

The look-up table-based OCV, internal resistances, and discharge/charge PL within the battery pack model can be easily updated as new lithium-ion cell chemistries are developed for HEVs or battery electric vehicles. The data-driven battery pack model and mathematical rule-based VSC in the ALPHA and GT-DRIVE co-simulation vehicle models enable fuel economy and GHG emissions to be estimated by optimizing various battery pack design variables, SOC operating windows, BMS cooling strategies, battery pack power, and pack energy capacity.

Co-simulations of GT-DRIVE and the ALPHA vehicle model can be used to optimize lithium-ion battery pack design parameters to meet vehicle electrification power demand by implementing a two-time constant equivalent circuit battery cell model, a lumped battery thermal model, and typical MHEV VSC and BMS control strategies. The 48V lithium-ion battery pack model was validated with HIL battery test data generated at the EPA NVFEL battery test laboratory in Ann Arbor and using 2013 GM Chevrolet Malibu Eco MHEV chassis dynamometer test data generated by ANL.

## Contact Information

### SoDuk Lee

Ph.D. Assessment & Standards Division  
US EPA - Office of Transportation & Air Quality  
2000 Traverwood Drive, Ann Arbor, MI 48105  
Phone: 734-214-4373  
[lee.soduk@epa.gov](mailto:lee.soduk@epa.gov)

## Disclaimer

This document has been reviewed in accordance with U.S. EPA policy and approved for publication. The views expressed in this article are those of the authors and do not necessarily reflect the views or policies of the U.S. EPA.

## Acknowledgments

The authors would like to acknowledge the following persons for their cooperation to this model development and validation:

- Eric Rask, Michael J. Duoba, Kevin Stutenberg, and Henning Lohse-Busch at ANL for sharing chassis dynamometer test data.
- Tim Burress at Oak Ridge National Laboratory for providing electric motor efficiency test data.
- Mr. Joseph Wimmer and Ryan Tooley at Gamma Technologies for their extensive technical support with GT-DRIVE.

## Abbreviations/Definitions

**ALPHA** - Advanced Light-Duty Powertrain and Hybrid Analysis

**ANL** - Argonne National Laboratory

**BSA** - Belt starter-alternator

**BTF** - Battery test facility

**BISG** - Belt integrated starter generator

**BMS** - Battery management system

**DLL** - Dynamic link library

**DPL** - Discharge power limit

**EPA** - U.S. Environmental Protection Agency

**GEM** - Greenhouse Gas Emissions Model

**GHG** - Greenhouse gas

**HEV** - Hybrid electric vehicle

**HIL** - Hardware-in-the-loop

**HwFET** - Highway fuel economy test procedure

**ISA** - Integrated starter-alternator

**LD** - Light duty

**MHEV** - Mild hybrid electric vehicle

**MPV** - Multi-purpose vehicle

**NVFEL** - National Vehicle and Fuel Emissions Laboratory

**OCV** - Open-circuit voltage

**OEM** - Original equipment manufacturer

**PHEV** - Plug-in hybrid electric vehicle

**PID** - Proportional-integral-derivative

**RC** - Resistance-capacitance

**RMS** - Root mean square

**SOC** - State of charge

**UDDS** - Urban dynamometer driving schedule

**VSC** - Vehicle supervisory control

$\tau_{ST}/\tau_{LT}$  - Short-/long-time constant

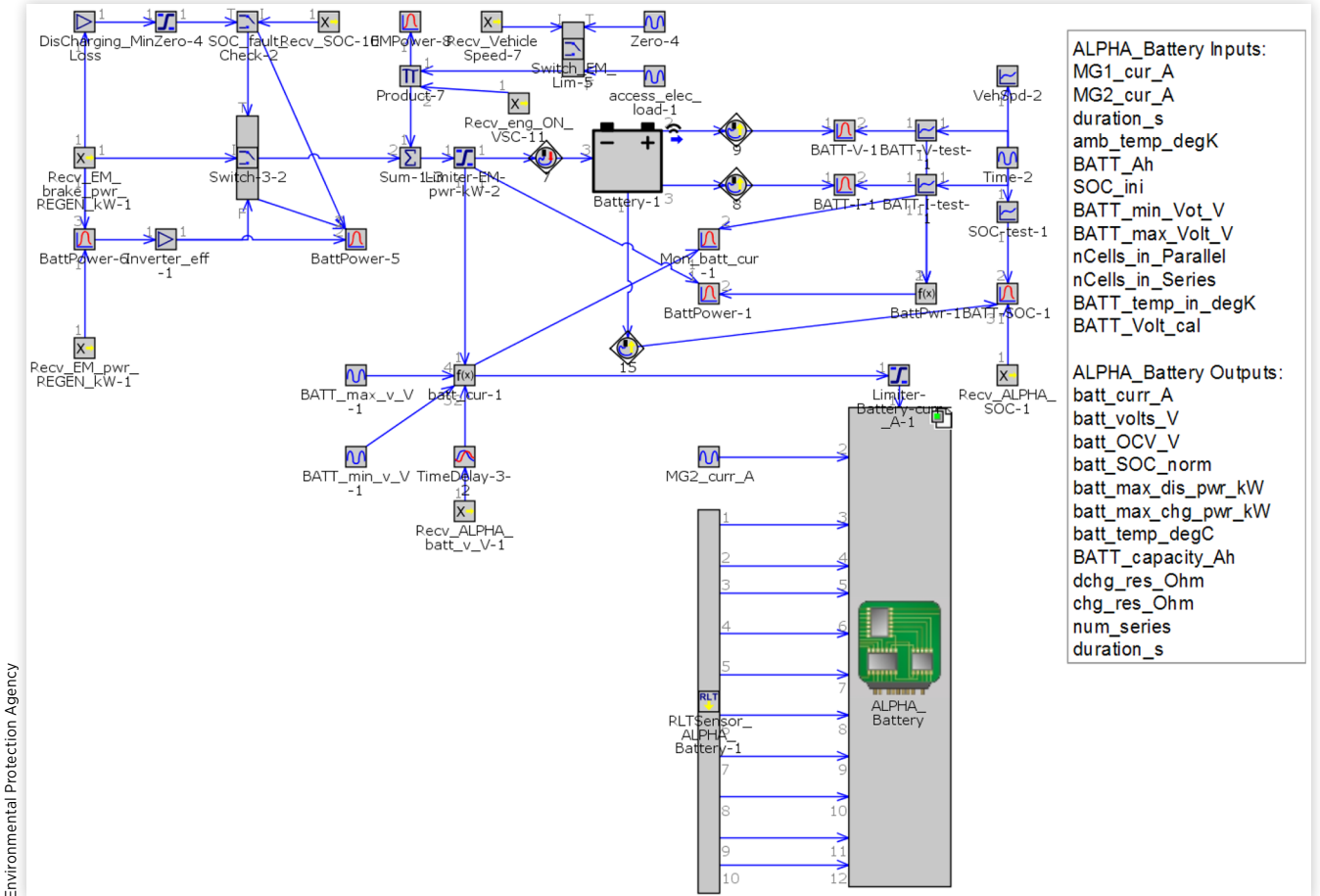
# References

---

1. Kelly, J., Scanes, P., and Bloore, P., "Specification and Design of a Switched Reluctance 48V Belt Integrated Starter Generator (B-ISG) for Mild Hybrid Passenger Car Applications," SAE Technical Paper [2014-01-1890](#), 2014, doi:[10.4271/2014-01-1890](#).
2. Pothin, R. and Dolcini, P., "Deployment of 48V in Renault, Current Status and Future Outlook," *Proceedings-Internationaler Motorenkongress*, Springer Vieweg, Wiesbaden, 2017.
3. Kemmler, R., Kreitmann, F., Werver, M., and Inderka, R., "M 264-The New Mercedes-Benz 4-Cylinder Toptype-Gasoline Engine with 48V-Electrification," *38th International Vienna Motor Symposium*, 2017.
4. Vollrath, O., Banken, J., Lautenschütz, P., and Storz, O., "M 256-The New Mercedes-Benz High-Performance Six-Cylinder In-Line Gasoline Engine with Intelligent 48V Electrification," *38th International Vienna Motor Symposium*, 2017.
5. Jablonowski, C., Schimmel, C., and Underberg, V., "The Chassis of the All-New AUDI A8," *Proceedings-8th International Munich Chassis Symposium*, Springer Vieweg, Wiesbaden, 2017.
6. Zoia, D.E., "FCA Makes Big Commitment to Electrification," Wards Auto, <https://www.wardsauto.com/engines/fca-makes-big-commitment-electrification>, June 1, 2018.
7. Lee, B., Lee, S., Cherry, J., Neam, A. et al., "Development of Advanced Light-Duty Powertrain and Hybrid Analysis Tool (ALPHA)," SAE Technical Paper [2013-01-0808](#), 2013, doi:[10.4271/2013-01-0808](#).
8. Lee, S., Lee, B., Zhang, H., Sze, C. et al., "Development of Greenhouse Gas Emissions Model for 2014-2017 Heavy- and Medium-Duty Vehicle Compliance," SAE Technical Paper [2011-01-2188](#), 2011, doi:[10.4271/2011-01-2188](#).
9. U.S. Department of Energy-Office of Energy Efficiency and Renewable Energy-Vehicle Technology Office, "Advanced Vehicle Testing Activity Data and Results," <https://energy.gov/eere/vehicles/advanced-vehicle-testing-activity-avta-data-and-results>, Dec. 2017.
10. U.S. Department of Energy-Office of Energy Efficiency and Renewable Energy-Vehicle Technology Office, "AVTA: 2013 Chevrolet Malibu HEV Testing Results," <https://energy.gov/eere/vehicles/downloads/avta-2013-chevrolet-malibu-hev-testing-results>, Dec. 2017.
11. Argonne National Laboratory, "2013 Chevrolet Malibu Eco," from the Downloadable Dynamometer Database, <http://www.anl.gov/energy-systems/group/downloadable-dynamometer-database/hybrid-electric-vehicles/2013-chevrolet>, Dec. 2017.
12. Schweighofer, B., Raab, K.M., and Brasseur, G., "Modeling of High Power Automotive Batteries by the Use of an Automated Test System," *IEEE Transaction on Instrumentation and Measurement* 52(4):1087-1091, 2003, doi:[10.1109/TIM.2003.814827](#).
13. Chen, M. and Rincon-Mora, G.A., "Accurate Electrical Battery Model Capable of Predicting Runtime and I-V Performance," *IEEE Transaction on Energy Conversion* 21(2):504-511, 2006, doi:[10.1109/TEC.2006.874229](#).
14. Lee, S., Lee, B., McDonald, J., and Nam, E., "Modeling and Validation of Lithium-Ion Automotive Battery Packs," SAE Technical Paper [2013-01-1539](#), 2013, doi:[10.4271/2013-01-1539](#).
15. Lee, S., Lee, B., McDonald, J., and Safoutin, M., "HIL Development and Validation of Lithium-Ion Battery Packs," SAE Technical Paper [2014-01-1863](#), 2013, doi:[10.4271/2014-01-1863](#).
16. Pesaran, A.A., "Battery Thermal Models for Hybrid Vehicle Simulations," *Journal of Power Sources* 110(2):377-382, 2002, doi:[10.1016/50378-7753\(02\)00200-8](#).
17. Pesaran, A.A. and Keyser, M., "Thermal Characteristics of Selected EV and HEV Batteries," *Annual Battery Conference: Advances and Applications*, Long Beach, California, January, 2001.
18. Ismail, N., Toha, S., Azubir, N., Izhak, N. et al., "Simplified Heat Generation Model for Lithium Ion Battery Used in Electric Vehicle," *IOP Conf. Series: Materials Science and Engineering* 52:012014, 2013, doi:[10.1088/1757-899X/53/1/012014](#).
19. Catherino, H.A., "Estimation of the Heat Generation Rates in Electrochemical Cells," *Journal of Power Sources* 239(1):505-512, 2013, doi:[doi.org/10.1016/j.powrsour.2013.03.169](#).
20. U.S. Code of Federal Regulations, Title 40, Part 86, § 86.158-00, 2000.
21. Lee, S., Cherry, J., Safoutin, M., McDonald, J. et al., "Modeling and Controls Development of 48V Mild Hybrid Electric Vehicles," SAE Technical Paper [2018-01-0413](#), 2018, doi:[10.4271/2018-01-0413](#).
22. Rask, E., Duoba, M., Lohse-Busch, H., and Walsh, P., "Advanced Technology Vehicle Lab Benchmarking-Level 2 (In-Depth)," presentation at the 2012 U.S. Department of Energy Hydrogen Program and Vehicle Technologies Annual Merit Review.
23. Lohse-Busch, H., "Advanced Technology Vehicle Lab Benchmarking-Level 1," presentation at the 2013 U.S. Department of Energy Hydrogen Program and Vehicle Technologies Annual Merit Review.

# A. Appendix

**FIGURE A.1** Schematic of the GT-Suite Battery and ALPHA Battery Model DLL.



Environmental Protection Agency

## B. Ohmic Series, Short- and Long-Time Resistances, Time Constants, and Capacitances of 48V Battery

---

```
batt_cur_chg= [200 100 50 25 10 5];  
batt_cur_dchg= [300 200 100 50 25 10 5];  
batt_soc = [30 35 40 45 50 55 60 65 70 75 80]; % some SOC values are inter/  
extrapolated
```

```
R_s_chg = [6.38 8.41 9.20 9.98 9.52 9.66 9.81 9.29 8.78 8.24 7.74  
4.96 5.31 5.81 5.86 5.92 7.35 8.77 5.20 4.90 4.60 4.32  
6.92 5.92 5.70 5.47 6.02 7.53 9.04 9.07 9.10 6.88 4.66  
8.28 7.08 7.80 8.52 8.84 9.16 9.16 9.16 5.08 5.14 5.20  
8.30 7.10 7.05 7.00 7.85 8.70 7.95 7.20 8.20 9.20 8.70  
8.18 7.00 6.50 6.00 6.90 7.80 7.40 7.00 8.00 9.00 8.40];
```

```
R_st_chg = [5.89 4.73 3.57 4.16 4.76 7.28 9.81 9.29 8.78 8.24 7.39  
6.53 6.17 7.01 7.51 8.01 7.42 6.83 5.20 4.90 4.6 4.12  
6.24 7.23 8.22 8.76 9.30 8.54 7.78 8.44 7.66 6.88 4.66  
5.88 5.55 6.31 6.72 7.64 8.56 8.58 8.60 5.08 5.14 5.2  
7.42 7.00 7.40 7.80 8.35 8.90 9.55 9.38 9.20 8.81 8.22  
7.85 7.40 8.70 10.00 10.00 10.00 9.90 9.80 9.40 9.00 8.40];
```

```
R_lt_chg = [3.84 3.06 2.27 2.65 3.02 2.62 2.40 3.43 6.20 5.73 6.22  
3.48 4.02 4.56 4.99 5.41 4.98 4.55 6.51 6.05 5.60 6.07  
4.04 4.67 5.30 5.70 6.10 5.63 5.16 5.42 5.68 6.20 6.72  
3.92 4.18 4.44 5.42 5.47 5.52 5.72 6.52 7.32 7.06 6.8  
4.78 5.10 5.30 5.50 5.55 5.60 6.40 7.20 6.70 6.20 6.00  
4.69 5.00 4.80 4.60 5.00 5.40 6.80 8.20 6.90 5.60 6.70];
```

```
C_st_chg = [254.67 421.45 588.24 567.51 546.79 488.35 429.91 496.91 563.9097744 550.42 536.93  
178.76 140.13 185.45 198.84 212.23 333.06 453.88 230.46 261.37 255.20 249.02  
416.67 317.82 218.98 243.90 268.82 378.62 488.43 463.62 438.80 382.23 325.6704981  
595.24 543.15 491.07 464.53 481.78 455.61 471.99 488.37 274.82 305.68 336.5384615  
485.32 442.86 420.15 397.44 412.20 426.97 404.66 382.35 422.88 463.41 481.71  
444.28 405.41 402.70 400.00 385.00 370.00 348.27 326.53 391.04 455.56 452.78];
```

```
C_lt_chg = [2109.38 2681.06 3252.75 2770.65 2288.56 2193.84 2099.13 1986.16 1873.198847  
1810.04 1717.32  
1841.23 1842.11 1690.76 1524.10 1497.23 1473.89 1450.55 1152.07 1114.50 1076.923077 1021.76  
1757.43 1624.00 1490.57 1343.64 1196.72 1170.07 1143.41 1091.07 1038.73 988.12 937.5  
1581.63 1511.54 1441.44 1376.23 1302.50 1068.84 1015.19 961.54 915.30 913.53 911.7647059  
1374.65 1313.73 1256.86 1200.00 1135.71 1071.43 945.44 819.44 885.53 951.61 941.32  
1423.07 1360.00 1299.57 1239.13 1184.38 1129.63 967.25 804.88 902.44 1000.00 897.44];
```

```
R_s_dchg = [8.55 8.67 8.79 8.81 8.83 7.83 4.79 5.67 6.55 5.60 4.66  
5.24 7.77 7.64 7.51 7.00 6.50 8.28 6.46 4.64 3.97 3.30  
8.63 8.46 8.29 6.24 5.56 4.88 5.52 6.16 4.42 3.78 3.15  
8.73 8.01 5.78 6.08 6.38 6.21 6.04 6.74 4.84 4.14 3.44  
8.98 8.40 6.40 7.32 8.24 8.08 7.92 8.84 6.34 5.43 4.51  
8.47 9.20 8.20 8.25 8.30 8.05 7.80 8.70 6.25 5.35 4.45  
8.75 8.90 7.00 7.80 8.60 8.34 8.08 9.02 6.47 5.54 4.61];
```

```
R_st_dchg = [4.83 4.69 4.54 4.32 4.09 5.03 5.98 5.43 4.88 5.45 6.03  
7.59 6.40 5.21 5.71 5.405 5.10 4.00 5.27 6.54 7.31 8.08  
7.20 6.78 6.60 6.41 6.71 7.00 6.52 6.04 7.50 8.38 9.26  
7.70 7.50 7.30 7.06 6.82 6.65 6.48 6.00 7.45 8.33 9.21  
8.64 7.98 7.32 6.76 6.20 5.90 5.60 5.19 6.44 7.20 7.96  
8.50 7.20 5.90 6.05 6.20 6.60 7.00 6.48 8.05 9.00 9.95  
8.20 7.40 6.60 6.40 6.20 5.90 5.60 5.19 6.44 7.20 7.96];
```

```

R_lt_dchg = [3.16 3.07 2.97 2.81 2.65 3.18 3.71 3.40 3.08 3.56 4.033333333
5.02 4.19 3.35 3.72 3.51 3.30 2.51 3.42 4.34 2.53 5.68
4.68 4.37 4.21 4.05 4.36 4.68 4.28 3.88 3.83 2.86 5.01
5.30 5.06 4.82 4.71 4.60 4.43 4.26 3.90 3.81 2.88 4.99
5.32 5.06 4.80 4.66 4.52 4.46 4.4 3.77 3.94 2.79 5.15
5.40 5.10 4.80 4.55 4.30 4.20 4.1 4.05 3.67 2.99 4.80
6.00 5.60 5.20 4.80 4.40 3.80 3.2 5.19 2.86 3.83 3.75];
C_st_dchg = [621.12 685.01 748.90 692.30 635.70 418.18 346.41 274.63 274.25 273.86
199.1150442
223.98 380.70 537.43 381.53 225.62 425.31 625.00 427.18 229.3577982 229.03 166.52
434.46 501.47 453.55 405.62 324.24 242.86 303.55 364.2384106 195.56 195.29 141.99
467.53 418.70 369.86 382.88 395.89 390.85 385.8024691 462.94 248.56 248.21 180.46
486.11 454.80 423.50 477.88 532.26 560.77 589.2857143 707.11 379.65 379.12 275.65
482.35 563.21 644.07 580.10 516.13 536.64 557.1428571 668.54 358.95 358.44 260.61
439.02 499.82 560.61 578.69 596.77 637.67 678.5714286 814.24 437.18 436.56 317.41];
C_lt_dchg = [2120.25 2136.36 2152.47 2433.02 2713.57 2516.86 2320.14 2457.37 2594.59 2363.41
2132.231405
1611.94 1850.75 2089.55 2071.67 2053.79 2461.16 2868.53 2390.48 1912.442396 1742.04 1571.64
1435.08 1464.53 1621.15 1777.78 1743.59 1709.40 1834.08 1958.762887 1567.06 1427.43 1287.80
1169.81 1311.05 1452.28 1487.01 1521.74 1617.68 1713.615023 1830.11 1464.13 1333.67 1203.22
1052.63 1224.23 1395.83 1405.88 1415.93 1435.24 1454.545455 1553.43 1242.78 1132.04 1021.31
1055.56 1142.36 1229.17 1370.40 1511.63 1463.13 1414.634146 1510.80 1208.68 1100.98 993.29
1033.33 1093.59 1153.85 1258.74 1363.64 1603.69 1843.75 1969.09 1575.32 1434.95 1294.59];

tau_st_chg = R_st_chg .* C_st_chg /1000;
tau_lt_chg = R_lt_chg .* C_lt_chg /1000;
tau_st_dchg = R_st_dchg .* C_st_dchg /1000;
tau_lt_dchg = R_lt_dchg .* C_lt_dchg /1000;

```

